

Conductive inks of graphitic nanoparticles from a sustainable carbon feedstock



Ferdinand Hof^{a, b, 1}, Katerina Kampioti^{a, b, 1}, Kai Huang^{a, b, 1}, Christèle Jaillet^{a, b},
Alain Derré^{a, b}, Philippe Poulin^{a, b}, Hisham Yusof^c, Thomas White^c, Krzysztof Koziol^c,
Catharina Paukner^{c, **}, Alain Pénicaud^{a, b, *}

^a CNRS, Centre de Recherche Paul Pascal (CRPP), UPR 8641, F-33600 Pessac, France

^b Université de Bordeaux, CRPP, UPR 8641, F-33600 Pessac, France

^c FGV Cambridge Nanosystems, CB5 8HY Cambridge, United Kingdom

ARTICLE INFO

Article history:

Received 14 June 2016

Received in revised form

8 September 2016

Accepted 22 September 2016

Available online 22 September 2016

ABSTRACT

Microwave plasma splitting of biogas to solid carbon forms is a promising technique to produce large quantities of sustainable carbon based nano materials. Well defined graphitic nano carbons have been produced exhibiting graphene multilayers in turbostratic packing. After heat treatment, the purified material has been used to formulate stable, aqueous dispersions. These dispersions are used directly as inks, allowing the preparation of conductive membranes with remarkable resistivity. Nano carbons derived by plasma processes constitute a promising alternative to carbon black because they can be prepared from renewable sources of methane or natural gas, are calibrated in size, exhibit high conductivity, and have promising perspectives for chemical and material science purposes.

© 2016 The Authors. Published by Elsevier Ltd. This is an open access article under the CC BY license (<http://creativecommons.org/licenses/by/4.0/>).

1. Introduction

The element carbon, with its rich family of allotropes, lately also on the nanometer scale, has attracted a broad interest resulting in a remarkable number of publications and patents [1]. In particular, the promising and extraordinary properties of graphene have triggered extensive research in various fields of science as well as economic and industrial interest in recent years [2,3]. Carbon black on the other hand is an essential, industry relevant product [4], which is ubiquitous in countless applications such as reinforcing filler for tires and other rubber goods, as a pigment for printing inks, coatings, conductive inks, plastics, etc. Depending on the application, different grades, qualities and grain sizes are available [5,6]. However, in the uttermost cases the chemical structure is inhomogeneous [7], not only in respect to the sp^2 to sp^3 carbon ratio but also in terms of heteroatom content [8,9]. These carbons are produced primarily by a feedstock from the petrochemical

industry. One important, modern challenge is the sustainable production of chemical products that does not rely only on petrochemical sources. Renewable methane, generated by anaerobic digestion of food waste fulfills that purpose. The as-produced biogas is nowadays mainly used for energy production. However, it is also a renewable source of hydrogen [10] and simultaneously an interesting feedstock for the production of sustainable graphitic nano carbons. By utilizing plasma processes, a variety of different carbon allotropes can be produced from hydrocarbons, such as fullerenes, carbon nanotubes and small graphitic nano carbons [11–14]. Depending on the type of feed gas, the presence of additives such as CO_2 or carrier gases e.g. helium, and the exact gas compositions, the yield of the generated carbon, the selectivity of the process, and the power consumption can be fine - tuned [15–17].

In this article, nanocarbons produced by a cold microwave plasma have been used to produce inks and conductive coatings. A detailed characterization of the starting materials and the inks has been performed. The carbon nanoparticles are composed of nano graphitic sheets, exhibiting 20–30 graphene layers and a lateral size of 30–80 nm. Membranes prepared with the corresponding inks show resistivities as low as $1 \Omega \text{ cm}$, i.e. in the range of high quality conductive grade carbon black. Therefore, generating large quantities of sustainable graphitic nano carbons appears to be

* Corresponding author. CNRS, Centre de Recherche Paul Pascal (CRPP), UPR 8641, F-33600 Pessac, France.

** Corresponding author.

E-mail addresses: cp@cnanos.com (C. Paukner), penicaud@crpp-bordeaux.cnrs.fr (A. Pénicaud).

¹ These authors contributed equally to the work.

feasible and technologically relevant. Due to their intrinsic size and defined chemical structure, the nano carbons described here can be directly used to formulate conductive inks with superior conductive properties. Therefore, these materials fit well between graphene and carbon black and constitute a promising and exciting alternative to established carbon blacks due to their well-defined nature, conductivity performances, and sustainability.

2. Experimental section

2.1. Material synthesis and heat treatment procedure

Five different nano carbon samples under study have been produced by FGV Cambridge Nanosystems using biogas reactor microwave plasma technology to cleave a methane/CO₂ mix (cf Table 1) into graphitic carbon and hydrogen. The power supply was kept constant at 6 kW. The flux of the feed gas into the biogas plasma reactor was kept constant at 20 l/min. The solid carbon products have been collected after 20 min of reaction time.

The purification of the nanocarbons was achieved by using controlled heat treatment, after taking into consideration the thermogravimetric analysis (TGA) results and adjusting the parameters. The heat treatment was conducted in a Nabertherm oven under air atmosphere with a heating slope of 5 °C/min until 500 °C. After a 6 h plateau, the oven was cooled at a rate of 5 °C/min down to 30 °C. The five heat treated nano carbons are accordingly called, NC_{HT0} - NC_{HT4}.

2.2. Physicochemical characterization

Raman spectroscopy. Raman spectroscopic characterization was carried out on a Horiba Jobin Yvon Xplora microscope equipped with a cooled Andor CCD detector; excitation wavelength: 532 nm, calibration on SiO₂, laser spot size of ~1 μm, 1200 lines per mm grating, objective Olympus 50× LWD. Raman mappings were performed with a motorized x-y μm scanning table. 1681 individual spectra were recorded on each sample. Calculations were performed using LabSpec6 and Origin 9.2.

X-ray diffraction (XRD). XRD patterns were collected on a PANalytical X'pert MPD-PRO Bragg-Brentano θ-θ geometry diffractometer equipped with a secondary monochromator over an angular range of 2θ = 8–80°. Each acquisition lasted for 2 h and 5 min. The Cu-Kα radiation was generated at 45 KV and 40 mA (λ = 0.15418 nm). The samples were put on silicon wafer (“zero background”) sample holder and flattened with a piece of glass.

Thermogravimetric characterization (TGA). Thermogravimetric characterization was performed on a Setaram instrument equipped with a 2 balance setup for equilibration. About 10 mg of nano carbon sample was weighed in a Pt-crucible. The measurement was performed under air.

Atomic force microscope (AFM). AFM images in ambient air were acquired using a Nanoscope III microscope operated in tapping mode using 8 nm radius tips MPP-111000.

Scanning tunneling microscope (STM). Ambient STM images were recorded on Nanoscope III microscope operated in STM mode using

Table 1

Synthesis condition and yields of the different graphitic nano carbons (NC) produced by the splitting of methane/CO₂ mix. The CO₂ concentrations have been varied from 0.0 vol% to 7.4 vol% in the feed gas into the 6 kW biogas plasma reactor to generate five different samples (0–4).

	NC ₀	NC ₁	NC ₂	NC ₃	NC ₄
CO ₂ (vol%)	0.0	0.4	1.7	4.9	7.4
Yield of carbon (g)	120	40.8	33.9	22.1	8.9

freshly cut platinum/iridium wire (Pt 80/Ir 20, 0.25 mm diameter).

2.3. Formulation of the dispersion

The aqueous dispersions of the heat treated nano carbons (NC_{HT0} - NC_{HT4}) were obtained with an optimized surfactant concentration and the aid of tip sonication. Typically, 320 mg of NC_{HT}, 50 mg of bile salt and 9.63 mL of H₂O were mixed and sonicated with a Branson Digital Sonifier tip sonicator for 30 min applying total energy E = 14.4 kJ in interval mode (pulse on: 0.5 s, pulse off: 0.2 s). Afterwards, the raw dispersion was centrifuged 20 min at 4000 rpm with a Fisher Bioblock Scientific centrifuge to remove the largest particles and aggregates. The final concentration of NC_{HT} is 17 mg mL⁻¹ (1.7 wt% NC_{HT}) with 5 mg mL⁻¹ (0.5 wt%) bile salt verified after weighing the freeze dried powder (yield 53%). The dispersions were used for the preparation of conductive films, optical measurements and AFM, STM measurements.

2.4. Resistivity measurements

The surface resistivity of nano carbon films was measured by a home-made four-point probe setup. Nano carbon films were obtained by the filtration of the dispersions on a membrane and drying under vacuum. Films were patterned by four gold contacts through a mask before resistivity measurement. The film thickness was measured by SEM (see Figs. S18 and S19, supporting information (ESI)). The measured I–V curves can be found in Fig. S20. The range of the resistivity measurements is between 0.01 μA up to 10 mA.

3. Results

The nano sized graphitic carbons were produced by the cracking of methane/CO₂ mix in carbon and hydrogen. The as produced five carbon samples were studied by thermal gravimetric analysis (TGA) from 20 to 750 °C under air (Fig. 1).

Three different areas of mass loss can be seen in the respective graph. Between 20 and 280 °C no mass losses are detectable. The first mass loss occurs between 280 and 500 °C with respective values of 5–11%. The highest mass loss is found for sample NC₄ and

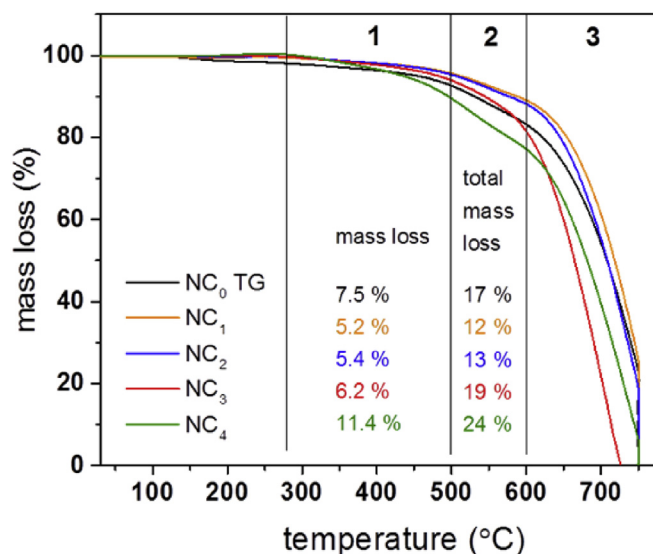


Fig. 1. TGA measurements under air between 20 and 750 °C. 3 different regions can be attributed that exhibit different mass losses. (A colour version of this figure can be viewed online.)

the least one in sample NC₁. In the second region, between 500 and 600 °C, roughly the same mass losses as mentioned above can be measured, doubling the total mass losses of the samples to 10–24%. The different samples are showing the same trend as in the first region. Beyond 600 °C, the samples are completely burned resulting in the complete loss of every sample. The ash contents of the samples were determined and the values are generally very low in the margin of less than 0.5 wt% (see also Table ST1, supporting information (ESI)).

3.1. Purification of the nano carbons

From the TGA measurements, a heat treatment procedure was designed to purify the materials. About 2 g of each nano carbon sample (NC) was annealed at 500 °C for 6 h (details see experimental section and ESI). The resulting weight losses of the purifying process were in agreement with the data gathered by TGA measurements exhibiting between 12 and 24% of weight losses for the five samples. The heat treated (HT) samples are named NC_{HT0} up to NC_{HT4}.

3.2. Solid material analysis

XRD studies have been performed to study the content of crystalline parts of the five carbon samples before (NC₀ – NC₄) and the five different carbon samples after heat treatment (NC_{HT0} – NC_{HT4}). The spectra after heat treatment are presented in Fig. 2, showing 3 different peaks at 2θ of ca 25.8°, 43°, and 54°. The respective spectra of the samples before heat treatment were virtually identical.

The peaks at ca 25.8° can be assigned to the (002) peak of graphite [18], which are rather broad with a FWHM of more than 1.6°, typically observed for nano sized graphitic carbons [19,20]. By using these FWHM values and applying the Scherrer equation, the crystalline sizes of the nano graphitic carbon have been found to be about 10 nm (Table ST2). The interplane distance is 0.345 nm, which is characteristic of turbostratic graphite [21]. The mentioned values of the mean crystalline sizes correspond to the stacking in the (002) plane, which allows the estimation of the number of carbon layers in the samples. Thus, values of about 30 layers of graphene can be determined, that are turbostratically stacked, i.e. there is no positional correlation between the layers. The peak at

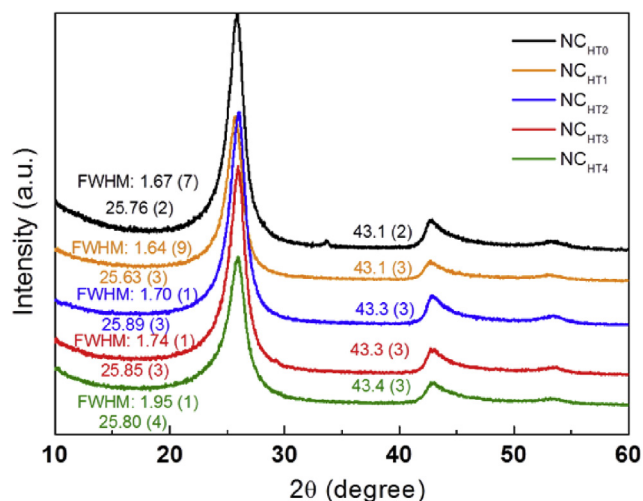


Fig. 2. XRD data of the five heat treated nano carbon samples. (A colour version of this figure can be viewed online.)

around 43° can be assigned to a convolution of the (100) and (101) peaks [18,22], allowing the determination of the in-plane domain size. The values are depicted in Table ST2 and are about 10 nm for the different NC. The XRD data of the non-purified material (Fig. S1 and Table ST2) exhibit practically identical values.

Raman spectroscopy has turned in recent years to be one of the most utilized technique to determine the quality of graphite as well as graphene [23–25]. Most important modes are the D, G and 2D mode [26]. The ratio between the area of the D and the G mode provides information about the sp³ to sp² carbon ratio. Due to the inhomogeneity of these carbon materials, statistical methods need to be applied in order to retrieve a comprehensive picture about the sample composition [27,28]. In this study, 1681 individual Raman spectra were recorded for each sample and in each spectrum the D and the G-mode were fitted by a Lorentzian function using Lab-Spec6. The resulting histograms of the heat treated samples are plotted in Fig. 3.

As can be clearly seen, the ratios of A_(D/G) values of all carbon samples exhibit Gaussian distributions with values in the range of 0.5–0.7 ± 0.1 to 0.6–0.8 ± 0.1. Likewise, G-mode line widths also follow Gaussian statistics with mean values of 39 cm⁻¹ up to 56 cm⁻¹ (Fig. 4).

The statistically derived values of 39–56 cm⁻¹ in comparison to the ones published by Ferrari et al. [29,30] and Caçado et al. [31] indicate that the crystalline domains of these carbon samples are in the region between 5 and 20 nm. Additional Raman data can be found in Figs. S2–S5. Ferrari et al. have classified disordered graphitic carbons from the least disordered (stage I) to the most disordered (stage III) with increasing amount of sp³ to sp² carbon atoms [29,30]. G-mode position, line width, and A_(D/G) allow classifying the nano carbons under study as stage II. Within this range an increase of order in the carbon lattice results in an increase of the D-mode, contrary to what is observed for less disordered graphitic materials [31]. G-line width decreases with ordering. From the insets of Figs. 3 and 4, it can be seen that the heat treated samples are more crystalline than the raw materials (higher A_(D/G) and lower G mode width).

By means of XPS measurements (Figs. S6–S8) element

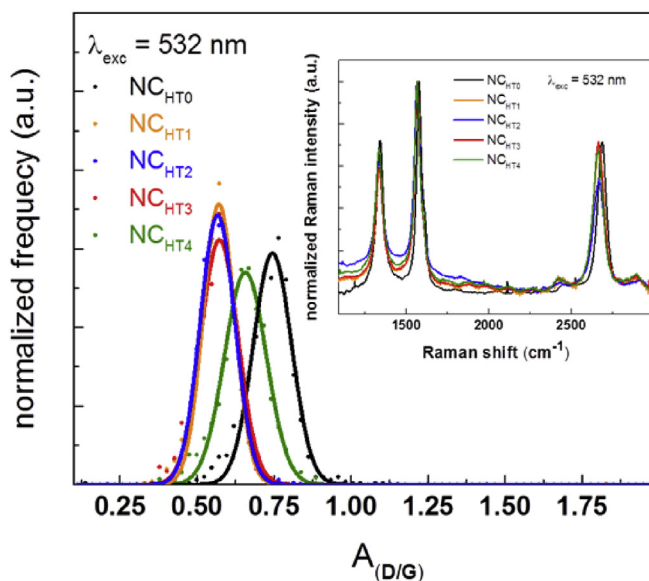


Fig. 3. Statistical Raman spectroscopy integrated intensities A_(D/G) value of the 5 nano graphite samples measured at 532 nm excitation wavelength. Inset: Raman mean spectra of the different samples (NC) after heat treatment. (A colour version of this figure can be viewed online.)

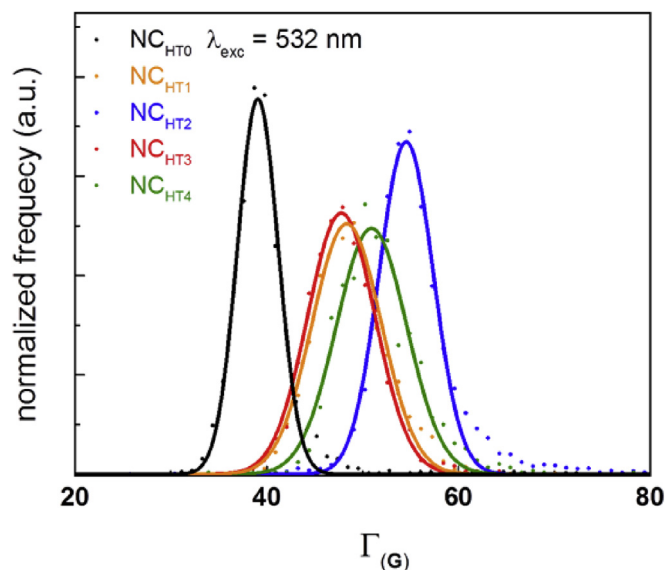


Fig. 4. Width of the G-mode extracted on a statistical basis of the respective samples after heat treatment. Raman spectra were measured at 532 nm excitation wavelength. (A colour version of this figure can be viewed online.)

concentrations and chemical binding environments can be determined. Peaks for carbon and oxygen can be found for each sample at 285 eV and 533 eV, respectively. The shape of the carbon peaks is rather broad and exhibit a broad tail. After heat treatment, the carbon peaks are sharper than before treatment. In contrast, differences in the tails of the samples before and after heat treatment are negligible. The tail of the carbon peak can be assigned to carbon that is bound to oxygen in different binding motifs. From XPS data (Table ST3), the carbon content of the sample can be estimated at more than 97%. As expected, the oxygen concentrations in the five different samples are slightly increased after the heat treatment procedure. By IR-spectroscopy (Fig. S9) the functional groups of these samples can be further characterized. The most prominent peaks are found at 2960–2840 cm^{-1} , 1574 cm^{-1} , 1368 cm^{-1} , 1062 cm^{-1} and around 3400 cm^{-1} . The peaks that can be found at 3400 cm^{-1} , 1368 cm^{-1} , and 1062 cm^{-1} can be attributed to COH, CO and COC vibrations. Furthermore, vibrations with small intensities between 2960 and 2840 cm^{-1} can be found in the respective spectra that can be attributed to alkylic C–H vibration. The rather intense peak at 1574 cm^{-1} fits nicely to the aromatic C=C vibration of the NC lattice. Further evidence of the presence of hetero atom contents in these NC samples can be found by elemental analysis (Table ST4).

The specific surface area is a critical value that provides information about the accessibility of the carbon framework. Specific area of samples NC₀₋₄ were obtained by means of BET measurements. They range between 141 m^2/g and 196 m^2/g (Table 2).

3.3. Dispersion of the purified nano carbons

To further evaluate the properties of these nano graphitic carbons the different heat treated carbon samples were dispersed with the aid of surfactant (bile salt) in water. By adjusting literature

procedures [32,33], optimized surfactant concentration of 0.5 wt% (5 mg mL^{-1}) bile salt have been used. The dispersions obtained, containing concentration of NC in aqueous up to ca 3.2 wt%. By fine tuning both sonication and centrifugation parameters, different compositions of sample sizes could be generated. After sonication, a centrifugation step of 2 min at 4000 rpm allowed generating a majority compound (2/3) with particles of ca 60 nm lateral sizes with 1/3 of other particles around 0.5 μm lateral size (see Figs. S10–S12). With further centrifugation treatment (20 min/4000 rpm), one size population was successfully isolated at around 60 nm (Figs. S10–S12).

The final nano carbon concentrations were verified by freeze drying of the five different NC_{HT} dispersions. Bimodal (2 min centrifugation) and monodisperse (20 min centrifugation) NC concentrations are 2.4 wt% and 1.7 wt%, respectively. The loss of material by centrifugation was 25% for the former and 47% for the latter. In order to characterize the aqueous dispersions, absorption spectra were taken in the UV/Vis region using a Unicam UV/Vis spectrometer UV4 (Fig. 5).

All absorption spectra exhibit a peak in the UV region at 264 nm except of NC_{HT4} which peak is found at 260 nm. This single absorption peak in the UV region is observed due to the linear dispersion of Dirac electrons in nano graphitic carbon. The peak at 264 nm is due to the collective π - π^* electronic transition of the condensed aromatic rings in the graphene sheet [34].

Atomic force microscopy is the method of choice to evaluate the size as well as the height of the carbon material in dispersion (Fig. 6).

Thus, 20 μl of the as-centrifuged dispersion were drop-casted on a freshly cleaved mica substrate. The resulting AFM topography image (Fig. 6a) of sample NC_{HT2} shows a very flat surface bearing homogenous nano-objects characterized by a height less than 3 nm (see full sized cross section in the inset). Individual objects can be clearly observed. Statistical analysis of the height distribution (Fig. 6b) gives a mean height of 3 nm for the nano carbons. The statistical analysis of the diameter distribution (Fig. 6c) shows a lateral size of ca 40 nm with a broad distribution from 30 to 80 nm.

Ambient STM experiment were also recorded for deposits from NC_{HT2} dispersion on HOPG (Fig. 7a), showing several nano carbon objects and a small region of aggregated objects but of similar form and shape than the individual ones. Two cross sections were plotted on several individual nano carbons (Fig. 7b and c). The size

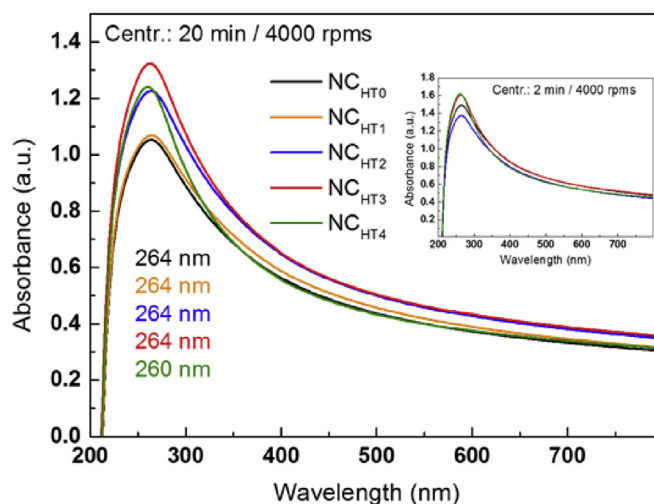


Fig. 5. Absorption spectra in the UV/Vis region of the different carbon samples after purification treatment with centrifugation treatment 2 min/4000 rpm and 20 min/4000 rpm. (A colour version of this figure can be viewed online.)

Table 2
Surface area (BET method) of the different graphitic nano carbons.

	NC ₁	NC ₂	NC ₃	NC ₄
BET (N ₂) m^2/g	153	141	158	196

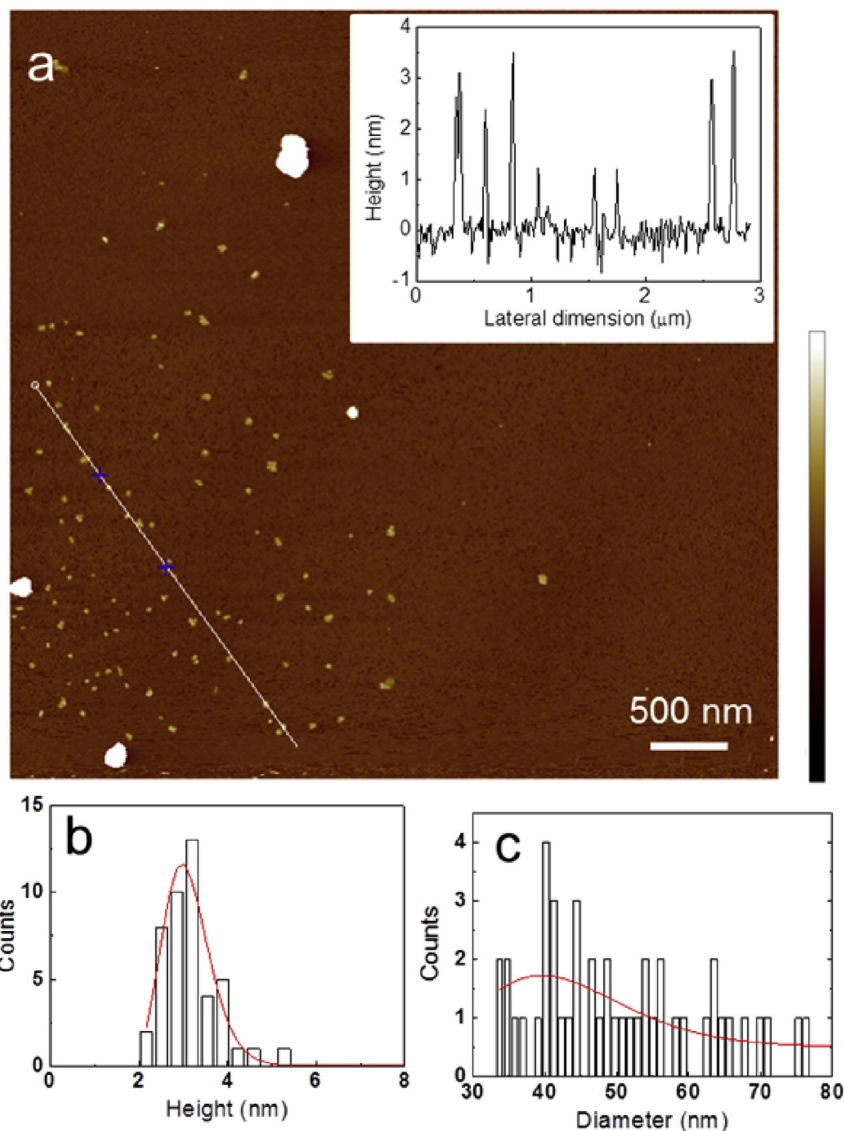


Fig. 6. (a) AFM topography image of deposits of nano carbon dispersion (NC_{HT2}) on freshly cleaved mica surface. Cross sections of the topography image taken along the white line are plotted in the inset. (b) Height distribution of nano carbons showing that the mean height of nano carbons is 3 nm. (c) Lateral size distribution of nano carbons showing that the mean size of nano carbons is 40 nm. (A colour version of this figure can be viewed online.)

of these objects range from 30 to 60 nm and their height vary from 0.4 to 1.6 nm. The AFM images of other carbon samples show sizes between 10 and 40 nm and similar heights as NC_{HT2} (see AFM images Figs. S13–S16).

TEM microscopic measurements were performed on each of the five dispersions. Representative images of NC_{HT2} can be found in Fig. 8, while the images of the other samples are presented in Fig. S17.

In Fig. 8 a,b, lower magnification HR-TEM images of the sample NC_{HT2} are presented. Here, the overall morphology of the aggregated carbons in the sample can be seen. In the higher magnification HR-TEM images Fig. 8 c,d the ordered domains within the bigger aggregates become visible and their size can be studied. The distance between the carbon layers can be determined and exhibits values of ca 0.34 nm. The lateral distance of the ordered regions of the sample exhibits values of about 10 nm.

3.4. Resistivity measurements

Resistivity measurements were performed on nano carbons

films prepared by filtration of nano carbon dispersions on a membrane, using a four probe measurement to give the sheet resistance (see S18 and material section). The film thicknesses were determined by means of SEM (see Fig. S19) providing the volume resistivity. The measured resistivities are all in the range of 0.5–1.5 Ω cm, but for one sample. The underlying I–V curves can be found in Fig. S20.

4. Discussion

Biogas derived from anaerobic digestion is an interesting feedstock for the production of sustainable, graphitic nano carbons. As a model case, methane/ CO_2 mix have been used to produce the nano carbons under study. The yield of the generated carbon is reversely depended on the CO_2 concentration during the biogas plasma process. From the TGA data, two conclusions can be drawn: i) the carbon lattice is stable under air up to 600 °C, above that temperature total burning of the carbon lattice occurs. ii) about 10–25% of the total mass can be removed by thermal treatment between 20 and 500 °C. Presumably, it is an amorphous part within the

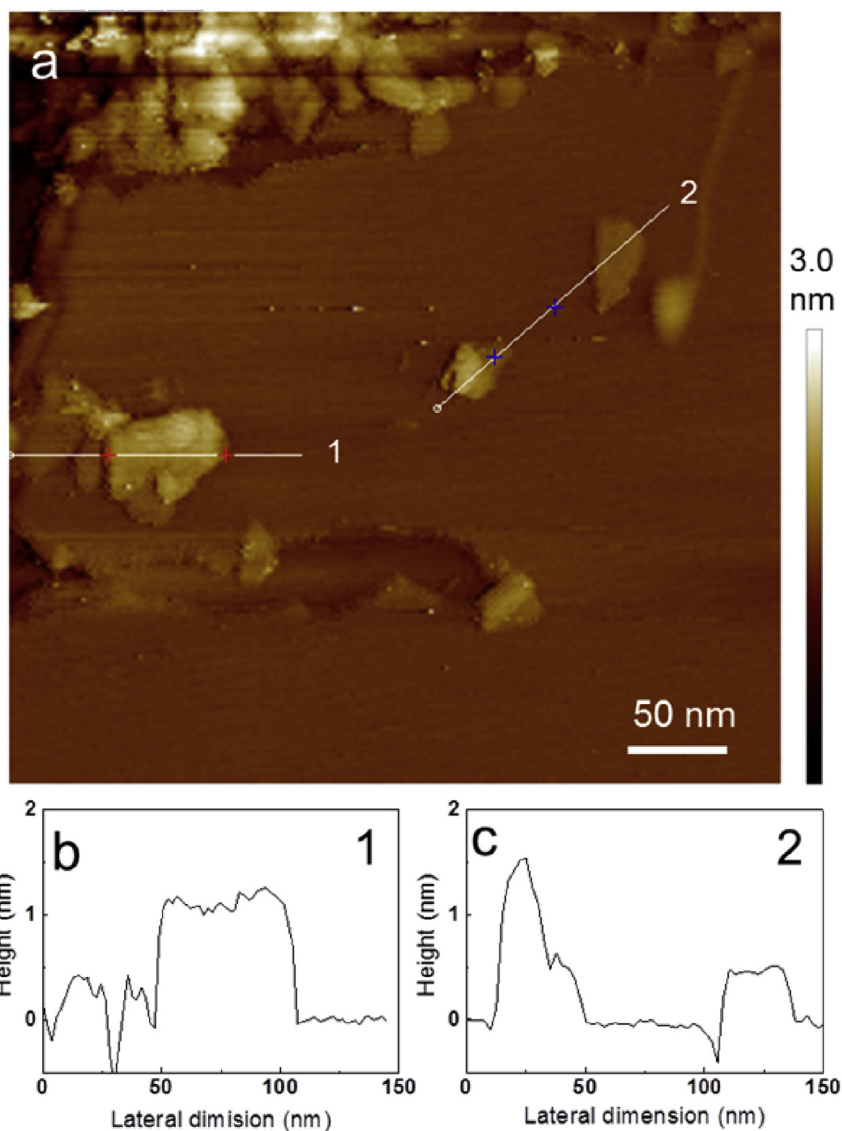


Fig. 7. (a) Ambient STM image of deposits of nano carbon dispersion (NC_{HT2}) on freshly cleaved HOPG surface. Several individual nano carbons and some nano carbon aggregations (top) are clearly seen. (b, c) Cross sections taken along the white lines 1 and 2. (A colour version of this figure can be viewed online.)

samples. The stability of the carbon lattice can be traced back to the graphitic nature of these nano carbons. This argument is further strengthened by XRD and Raman studies, as the graphitic nature of the carbons can be probed. An increase in the respective statistically obtained $A_{(D/G)}$ values is observable after heat treatment. In contrast to Raman spectra measured for pristine graphite or graphene, where the rise of the $A_{(D/G)}$ mode can be correlated to an increase of lattice defects, in these materials, an increased $A_{(D/G)}$ value corresponds to a less defective material (stage II compounds) [30]. The statistically determined mean widths of the G-modes of the different carbon materials of $40\text{--}55\text{ cm}^{-1}$ allow the estimation of the size of the graphitic domains to ca 5–20 nm. The XRD data presented in Fig. 2, show the presence of the (002) peak that can be related to about 10 nm of crystalline domains along the c axis which correspond to about 30 layers of turbostratically stacked graphene. The XRD data of the heat treated samples do not exhibit a big difference compared to the untreated material. These findings are in agreement with the successful removal of amorphous parts of the sample as predominantly only the graphitic parts of each sample are probed by this technique. The presence of amorphous parts

within these samples can be studied by means of XPS and IR spectroscopy. From the position and the shape of the C peak in the XPS measurements, it appears that the samples contain mainly sp^2 hybridized carbons. However, a significant amount of sp^3 hybridized carbon is present (about 40%). This value is reduced to 25% by heat treatment. Additionally, the presence of oxygen in several different C–O binding motives can be anticipated. It can be argued that the content of oxygen functional groups is very similar, before and after heat treatment, showing that the heat treatment predominantly removes amorphous parts of the sample rather than introducing defects in the graphitic layers. It has been shown by SLS and UV–Vis measurements that stable aqueous dispersions of calibrated size can be generated. Two size populations of the dispersions were obtained, corresponding to 79% of the starting dispersed material while monodispersed suspensions correspond to 53% of the initial dispersed material. By means of SLS, TEM, AFM and STM measurements the size of the dispersed objects can be studied. The particles exhibit a lateral size in the range between 30 and 60 nm and heights of 0.4–3.0 nm. The graphitic domains have been estimated at ca 5–20 nm. The defects can be attributed to

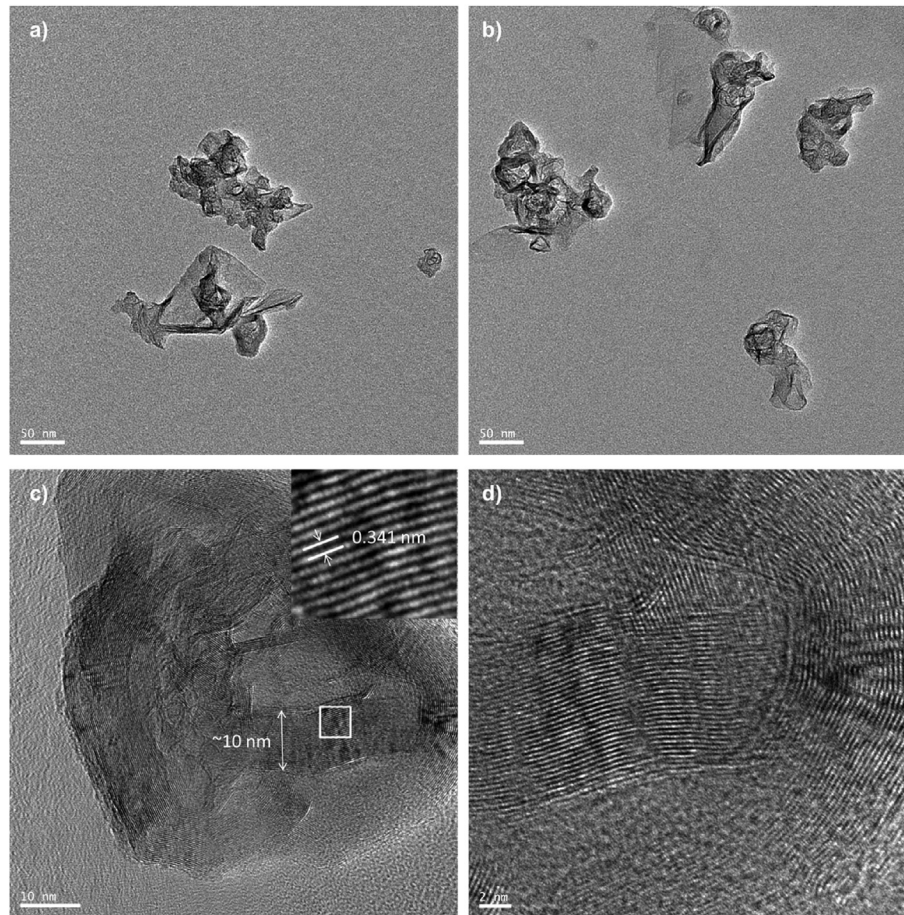


Fig. 8. Representative HR-TEM images of the nano carbon sample NC_{HT2} , showing the general morphology of the samples at lower magnification a,b (scale bar 50 nm) and the graphitic nature with higher magnification c,d (scale bar 10 and 2 nm) allowing the identification of ordered domains within the samples.

edges and point defects, as the determined graphitic domains and the flakes sizes are in the same order of magnitude. Thus, it can be argued that the carbon material derived by this biogas plasma process produces well defined, nano graphitic material. Therefore, it is very reasonable that conductive membranes can be made upon vacuum filtration. The Resistivity of NC_{HT0} and NC_{HT3} have been found to be about $1 \Omega \text{ cm}$ in the respective membranes. The actual shape of the carbon objects influences the respective resistivity dramatically, as have been shown by A. Celzard et al. [35]. Resistivity for different carbon forms have been found to exhibit

values of $0.02 \Omega \text{ cm}$ in membranes prepared from MWCNTs, $1.10 \Omega \text{ cm}$ for carbon black, and $0.08 \Omega \text{ cm}$ for graphite [36,37]. Thus, it can be argued that the determined values are in the range of high quality, conductivity grade carbon black (10^0 – $10^{-1} \Omega \text{ cm}$). Typically, the resistivity can be improved by either applying compression to the sample or by increasing the thickness of the sample. From Table 3, it is apparent that sheet resistance as low as $220 \Omega/\text{sq}$ can be found for thicknesses even below $25 \mu\text{m}$. This observation has technological relevance, opening the way to conductive coatings, electromagnetic shielding, and other conductivity related

Table 3
Volume resistivity of nano carbon films.

Sample	Trial	Thickness (μm)	Sheet resistance ($\text{k}\Omega/\text{sq}$)	Volume resistivity (Ωcm)	Average volume resistivity (Ωcm)
NC_{HT0}	1	19	0.90	1.7	2
	2	22	1.24	2.7	
	3	31	0.53	1.6	
NC_{HT1}	1	8	1.00	0.8	0.88
	2	31	0.36	1.11	
	3	49	0.15	0.74	
NC_{HT2}	1	15	0.21	0.32	0.39
	2	15	0.32	0.47	
	3	18	0.22	0.39	
NC_{HT3}	1	10	1.65	2.1	1.48
	2	41	0.34	1.4	
	3	46	0.21	0.96	
NC_{HT4}	1	12	42.0	50	34.4
	2	31	6.00	18.8	

applications.

5. Conclusion

The cracking of a methane/CO₂ mix by biogas microwave plasma yields multilayered graphitic particles in turbostratic packing motif. The raw material can be purified by heat treatment. For the best samples, ca 12% amorphous material is lost that way. The nano carbons can be dispersed in water with surfactant by sonication. A mild centrifugation step allows obtaining aggregate free mono-disperse suspensions bearing about 50 wt% of the initial carbon concentration. The size calibrated dispersion is made of particles of ca 30–80 nm in lateral size and 3 nm in thickness. Raman spectroscopy on a statistical basis shows that edges and point defects actually represent most if not all of the defects further underlining the quality of these materials. These nano carbons exhibit advantages to commercially available carbon black because they can be produced from a sustainable feedstock (biogas produced by anaerobic digestion). Aqueous inks with a narrow size distribution have been formulated. These inks have been used to generate conductive membranes that can be compared to ones made from high quality, conductivity grade carbon blacks. Additionally, due to the size of these graphitic nano carbons these are a very promising alternative as conductive fillers in polymers as well as for functional materials.

Acknowledgment

Funding from the European Union's Seventh Framework Program for research, technological development and demonstration under grant agreement No 603488 (Plascarb project) is acknowledged.

Appendix A. Supplementary data

Supplementary data related to this article can be found at <http://dx.doi.org/10.1016/j.carbon.2016.09.052>.

References

- [1] Y. Gogotsi, Not just graphene: the wonderful world of carbon and related nanomaterials, *MRS Bull.* 40 (2015) 1110–1121.
- [2] K.S. Novoselov, V.I. Fal'ko, L. Colombo, P.R. Gellert, M.G. Schwab, K. Kim, A roadmap for graphene, *Nature* 490 (2012) 192–200.
- [3] A.C. Ferrari, F. Bonaccorso, V. Falco, K.S. Novoselov, S. Roche, P. Bøggild, et al., Science and technology roadmap for graphene, related two-dimensional crystals, and hybrid systems, *Nanoscale* 7 (2014) 4598–4810, <http://dx.doi.org/10.1039/C4NR01600A>.
- [4] M. Voll, P. Kleinschmit, *Carbon*, 6. Carbon black, in: *Ullmann's Encycl. Ind. Chem.*, Wiley-VCH Verlag GmbH & Co. KGaA, Weinheim, Germany, 2010, pp. 23–44.
- [5] E. Alexander, C. Sommer, Systematic analysis of carbon black structures, *J. Phys. Chem.* 60 (1955) 1646–1649.
- [6] J.-B. Donnet, Fifty years of research and progress on carbon black, *Carbon N. Y.* 32 (1994) 1305–1310.
- [7] L. Fulcheri, N. Probst, G. Flamant, F. Fabry, E. Grivei, X. Bourrat, Plasma processing: a step towards the production of new grades of carbon black, *Carbon N. Y.* 40 (2002) 169–176.
- [8] H. Boehm, Surface oxides on carbon and their analysis: a critical assessment, *Carbon N. Y.* 40 (2002) 145–149.
- [9] H.P. Boehm, Some aspects of the surface chemistry of carbon blacks and other carbons, *Carbon N. Y.* 32 (1994) 759–769.
- [10] Y.N. Chun, Y.C. Yang, K. Yoshikawa, Hydrogen generation from biogas reforming using a gliding arc plasma-catalyst reformer, *Catal. Today* 148 (2009) 283–289.
- [11] J. Kang, O.L. Li, N. Saito, Synthesis of structure-controlled carbon nano spheres by solution plasma process, *Carbon N. Y.* 60 (2013) 292–298.
- [12] L. Juan, H. Fangfang, L. Yiwen, Y. Yongxiang, D. Xiaoyan, X. Liao, A new grade carbon black produced by thermal plasma process, *Plasma Sci. Technol.* 5 (2006) 1815–1819.
- [13] J. Gonzalez-Aguilar, M. Moreno, L. Fulcheri, Carbon nanostructures production by gas-phase plasma processes at atmospheric pressure, *J. Phys. D. Appl. Phys.* 40 (2007) 2361–2374.
- [14] A. Shashurin, M. Keidar, Synthesis of 2D materials in arc plasmas, *J. Phys. D. Appl. Phys.* 48 (2015) 314007.
- [15] K.S. Kim, J.H. Seo, J.S. Nam, W.T. Ju, S.H. Hong, Production of hydrogen and carbon black by methane decomposition using DC-RF hybrid thermal plasmas, *IEEE Trans. Plasma Sci.* 33 (2005) 813–823.
- [16] A. Indarto, J.W. Choi, H. Lee, H.K. Song, Effect of additive gases on methane conversion using gliding arc discharge, *Energy* 31 (2006) 2650–2659.
- [17] A. Indarto, N. Coowanitwong, J. Choi, H. Lee, H. Keun, Kinetic modeling of plasma methane conversion in a dielectric barrier discharge, *Fuel Process Technol.* 9 (2007) 8–13.
- [18] Z.Q. Li, C.J. Lu, Z.P. Xia, Y. Zhou, Z. Luo, X-ray diffraction patterns of graphite and turbostratic carbon, *Carbon N. Y.* 45 (2007) 1686–1695.
- [19] M.S. Paterson, Calculation of the correction for instrumental broadening in X-ray diffraction lines, *Proc. Phys. Soc. A* 63 (1950) 477–482.
- [20] N. Iwashita, C. Rae, H. Fujimoto, Specification for a standard procedure of X-ray diffraction measurements on carbon materials, *Carbon* 42 (2004) 701–714.
- [21] H. Fujimoto, Theoretical X-ray scattering intensity of carbons with turbostratic stacking and AB stacking structures, *Carbon N. Y.* 41 (2003) 1585–1592.
- [22] P.L. Walker, Measurement and crystal sizes of interlayer spacings carbons in turbostratic, *Carbon N. Y.* 1 (1963) 3–9.
- [23] A.C. Ferrari, D.M. Basko, Raman spectroscopy as a versatile tool for studying the properties of graphene, *Nat. Nanotechnol.* 8 (2013) 235–246.
- [24] A. Jorio, L.G. Cançado, Perspectives on Raman spectroscopy of graphene-based systems: from the perfect two-dimensional surface to charcoal, *Phys. Chem. Chem. Phys.* 14 (2012) 15246–15256.
- [25] R. Beams, L. Gustavo Cançado, L. Novotny, Raman characterization of defects and dopants in graphene, *J. Phys. Condens. Matter* 27 (2015) 083002.
- [26] M.A. Pimenta, G. Dresselhaus, M.S. Dresselhaus, L.G. Cançado, A. Jorio, R. Saito, Studying disorder in graphite-based systems by Raman spectroscopy, *Phys. Chem. Chem. Phys.* 9 (2007) 1276–1291.
- [27] S. Eigler, F. Hof, M. Enzelberger-Heim, S. Grimm, P. Müller, A. Hirsch, Statistical raman microscopy and atomic force microscopy on heterogeneous graphene obtained after reduction of graphene oxide, *J. Phys. Chem. C* 118 (2014) 7698–7704.
- [28] F. Hof, S. Bosch, J.M. Englert, F. Hauke, A. Hirsch, Statistical raman spectroscopy: a method for the characterization of covalently functionalized single-walled carbon nanotubes, *Angew. Chem. Int. Ed.* 51 (2012) 11727–11730.
- [29] A.C. Ferrari, J. Robertson, Raman spectroscopy of amorphous, nanostructured, diamond-like carbon, and nanodiamond, *Philos. Trans. A. Math. Phys. Eng. Sci.* 362 (2004) 2477–2512.
- [30] A. Ferrari, J. Robertson, Interpretation of Raman spectra of disordered and amorphous carbon, *Phys. Rev. B* 61 (2000) 14095–14107.
- [31] L.G. Cançado, A. Jorio, M.A. Pimenta, Measuring the absolute Raman cross section of nanographites as a function of laser energy and crystallite size, *Phys. Rev. B* 76 (2007) 064304.
- [32] L. Guardia, M.J. Fernández-Merino, J.I. Paredes, P. Solís-Fernández, S. Villar-Rodil, A. Martínez-Alonso, J.M.D. Tascón, High-throughput production of pristine graphene in an aqueous dispersion assisted by non-ionic surfactants, *Carbon N. Y.* 49 (2011) 1653–1662.
- [33] M. Lotya, Y. Hernandez, P.J. King, R.J. Smith, V. Nicolosi, L.S. Karlsson, M. Blighe, S. De, Z. Wang, I.T. MCGovern, G.S. Duesberg, J.N. Coleman, F.M. Blighe, Liquid Phase Production of Graphene by Exfoliation of Graphite in Surfactant/Water Solutions Liquid Phase Production of Graphene by Exfoliation of Graphite in Surfactant/Water Solutions, 2009, pp. 3611–3620.
- [34] G. Carotenuto, A. Longo, S. De Nicola, C. Camerlingo, L. Nicolais, A simple mechanical technique to obtain carbon nanoscrolls from graphite nanoplatelets, *Nanoscale Res. Lett.* 8 (2013) 403.
- [35] F. Payot, G. Furdin, A. Celzard, J.F. Mareche, Electrical conductivity of carbonaceous powders, *Carbon N. Y.* 40 (2002) 2801–2815.
- [36] B. Marinho, M. Ghislandi, E. Tkalya, C.E. Koning, G. De With, Electrical conductivity of compacts of graphene, multi-wall carbon nanotubes, carbon black, and graphite powder, *Powder Technol.* 221 (2012) 351–358.
- [37] J. Sánchez-González, A. Macías-García, M.F. Alexandre-Franco, V. Gómez-Serrano, Electrical conductivity of carbon blacks under compression, *Carbon N. Y.* 43 (2005) 741–747.